

Article

Towards an Integrated and Accurate Planktonic-Foraminiferal-Deduced Bio-Chrono-Stratigraphic Framework of Late Quaternary Mediterranean Marine Cores

George Kontakiotis *¹, Assimina Antonarakou¹, Evangelia Besiou, Elisavet Skampa¹ and Maria V. Triantaphyllou¹

Department of Historical Geology-Paleontology, Faculty of Geology and Geoenvironment, School of Earth Sciences, National and Kapodistrian University of Athens, Panepistimiopolis, Zografou, 15784 Athens, Greece; aantonar@geol.uoa.gr (A.A.); evabesiou@geol.uoa.gr (E.B.); elskampa@geol.uoa.gr (E.S.); mtriant@geol.uoa.gr (M.V.T.)

* Correspondence: gkontak@geol.uoa.gr

Abstract: The late Quaternary is a key stratigraphic interval as it encompasses the Late Glacial to Holocene transition, which is characterized by a series of pronounced centennial climate oscillations and subsequent short-term events of paleoceanographic variability. Across this stratigraphic interval, significant turnovers and faunal changes in the composition and abundance of planktonic foraminiferal assemblages are well-documented through their high-resolution quantitative analysis performed in the south Aegean core NS-18. The identification of 10 synchronous bioevents among the Mediterranean sub-basins allows accurate inter-basinal correlations over the study time interval, thus contributing to the development of a robust chronostratigraphic framework for this setting. Moreover, the identification and timing of additional 20 diachronous bioevents, in conjunction with the already established bio-ecozonation scheme of the Aegean Sea, provide a continuous record of faunal changes (in terms of species-specific distributional abundances) which can be used as an additional locally expressed biochronological tool for the eastern Mediterranean deep-sea cores. The present study certainly indicates that the cause-and-effect relationships between the paleoceanographic/paleoclimatic perturbations and biological response require a highly resolved regional chronostratigraphy.

Keywords: biochronology; integrated stratigraphy; synchronous and diachronous bioevents; inter-basinal sedimentary correlations; radiocarbon dating; centennial climatic changes; planktonic foraminiferal bio-ecozonation; late Quaternary evolutionary ecology; paleoceanography; eastern Mediterranean



Citation: Kontakiotis, G.; Antonarakou, A.; Besiou, E.; Skampa, E.; Triantaphyllou, M.V. Towards an Integrated and Accurate Planktonic-Foraminiferal-Deduced Bio-Chrono-Stratigraphic Framework of Late Quaternary Mediterranean Marine Cores. *J. Mar. Sci. Eng.* **2023**, *11*, 2345. <https://doi.org/10.3390/jmse11122345>

Academic Editors: Rosanna Maniscalco and Agata Di Stefano

Received: 17 November 2023
Revised: 7 December 2023
Accepted: 10 December 2023
Published: 12 December 2023



Copyright: © 2023 by the authors. Licensee MDPI, Basel, Switzerland. This article is an open access article distributed under the terms and conditions of the Creative Commons Attribution (CC BY) license (<https://creativecommons.org/licenses/by/4.0/>).

1. Introduction

The Mediterranean Sea is of particular importance to paleoceanography and paleoclimatology, as the marginal character of the basin promotes rapid responses to climate change, in such a way that any hydroclimate signal can be registered in an amplified fashion in its hydrological properties compared to the global oceans. Particularly, the Aegean Sea in its eastern sector is among the most studied basins due to its latitudinal position at the interface between the higher- and lower-latitude climate systems [1], and its heightened climate sensitivity because of the combination of its small size and semi-enclosed character due to the close atmospheric and partial isolated oceanic connections [2]. The peculiarities of this setting, mostly the large topographic contrasts, the oligotrophic nature, and the relatively small volume of the Aegean Sea, cause perturbations that can be recorded instantaneously in paleoceanographic data, such as microfossil abundances [3–8] and/or geochemical proxies [9–15]. Signals reflected by the changes in size, abundance, and/or distribution of the modern planktonic foraminiferal population have also been documented

for that basin [16–18], providing high-quality information, mostly related to their calcification, ecology, and related controlling factors [19–25], as well as comparative constraints at both the regional (entire Mediterranean basin; [26–29]) and global [30–32] scales. Moreover, the exceptionally high sedimentation rates reported for this basin (~20 cm/ky; [4,33–35]), compared to the open eastern Mediterranean (~4 cm/ky; [36]), provide a powerful tool for monitoring the paleoenvironmental conditions over the late Quaternary.

Geochronology is an essential tool in paleoceanographic studies aimed at providing an accurate chronostratigraphic framework of marine sediment cores through the combination of radiometric dating techniques (e.g., ^{14}C , ^{210}Pb , and ^{137}Cs), geochemical methods (e.g., stable oxygen isotopes $\delta^{18}\text{O}$; [37,38]), tephrostratigraphy [39–43], and micropaleontological datings (e.g., planktonic foraminiferal eco-biostratigraphic events; [44–50]). The application of high-resolution planktonic-foraminiferal-deduced biostratigraphic schemes, especially, during the late Quaternary has an exceedingly high potential for correlating (hemi)pelagic successions in several sub-basins (e.g., Siculo-Tunisian Strait [46,51], Tyrrhenian Sea [52–56], Adriatic Sea: [57–61], Mediterranean Ridge [62], Ionian Sea [63], Aegean Sea [3,6], and Levantine Sea [46]) across the entire Mediterranean Sea, owing to the continuously increasing and multidisciplinary nature of the planktonic foraminiferal contribution in biochronology (including biostratigraphy and bio-ecozonation). The concept of event stratigraphy enables the assembling of datings in considerable detail from high-sedimentation-rate cores, and, hence, provides guidance to the interpretation of the paleoclimatic data through stratigraphic correlations. The evidence of such high-resolution data facilitates inter-correlations between Mediterranean sub-basins and further offers a better comprehension of the paleoceanographic/paleoclimatic evolution of the entire Mediterranean region.

Within this context, this study carried out in a high-sedimentation-rate core retrieved from the southeastern Aegean emphasizes that the planktonic foraminiferal assemblages over the last glacial cycle provide useful insights to define biochronological events that can be used for the construction of an accurate chronostratigraphic framework both locally for the Aegean Sea and regionally for the eastern Mediterranean. The deglacial-to-Holocene period is an ideal time interval target for such an investigation because the sea level history is well-determined, the centennial scale chronostratigraphic resolution is highly achievable through planktonic foraminiferal eco-biozonation, and the paleoclimate history during that period is accurately constrained through previous studies [3,6,8,9,64]. The sapropel boundaries and the well-constrained bio-ecozonation scheme of Triantaphyllou et al. [3] for the study area further increase the accuracy of the planktonic foraminiferal stratigraphic ranges, thus improving the final biochronological scheme. Our micropaleontological dataset is strengthened by stratigraphically targeted accelerator mass spectroscopy (AMS) radiocarbon datings performed on planktonic foraminifera. Overall, the approach presented here is relatively simple and fast, and does not require highly professional skills or complicated instruments, and is mostly an inexpensive and non-time-consuming process. Such an integrated proxy could be considered a significant advance in the biostratigraphic structure of marginal settings, while it could also act as a template for future work on the late Quaternary by refining or extending previously established biostratigraphic schemes.

2. Regional Setting

The Aegean Sea is situated in the northeastern Mediterranean, between the Turkish and Greek coastlines (Figure 1). It is separated into two distinct (north and south Aegean) sub-basins with different hydrographic characteristics, which are controlled by the exchange of the Levantine and Black Sea water masses and subsequent climate contrasts between more humid conditions in the north and semi-arid conditions in the south [65]. It is one of the most oligotrophic areas in the world (especially its south basin; [66–69]) and is generally characterized by a cyclonic surface water circulation, supplemented by several permanent or transient mesoscale cyclonic and anticyclonic eddies [65,70,71]. The complex topography is another dynamic feature of the Aegean basin due to the great variability of its shores and bottom relief [72,73].

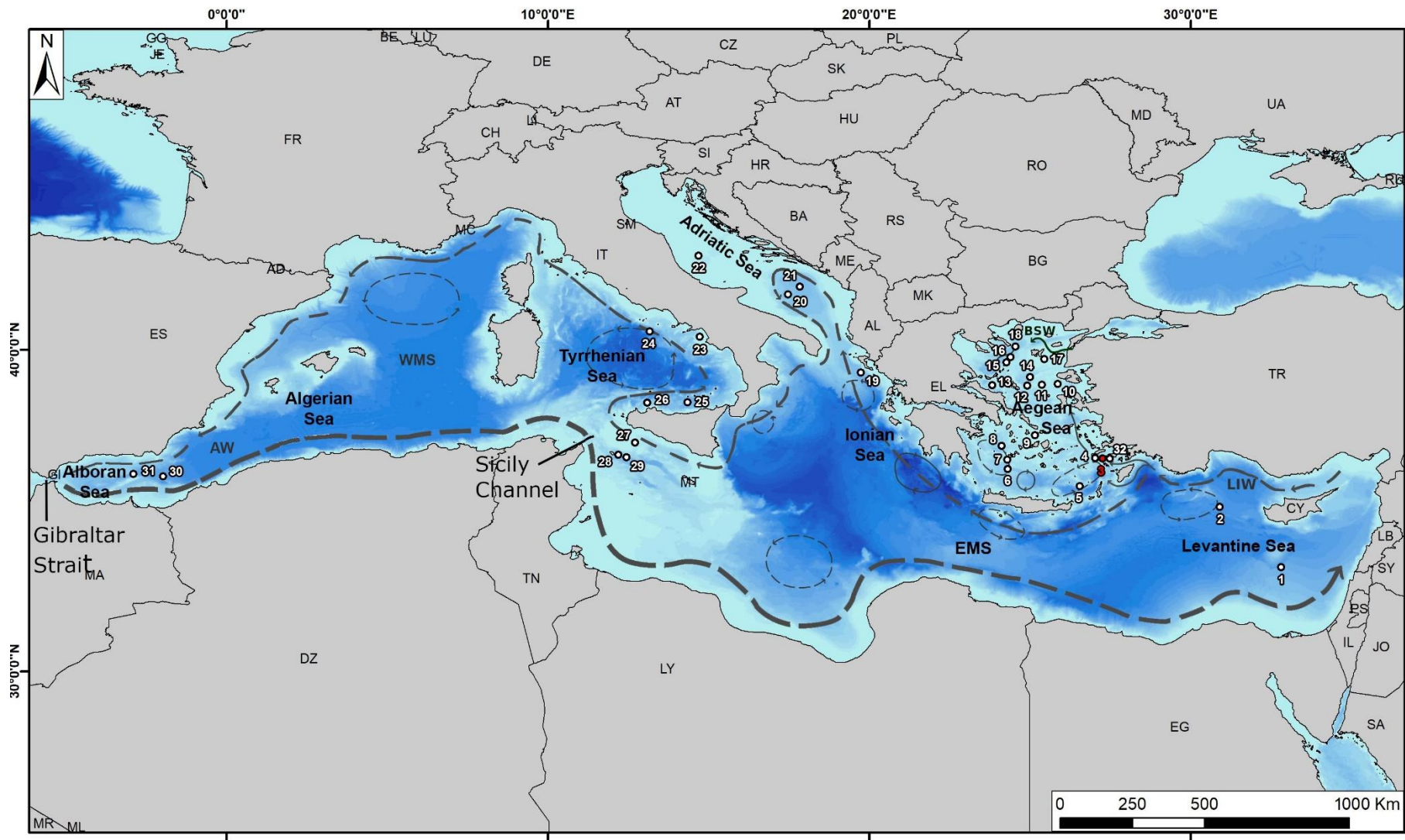


Figure 1. Bathymetric map of the Mediterranean Sea including surface oceanography and the location of the study core (numbered in red), as well as all the additional cores (numbered in white; Appendix A) used for comparison in different sub-basins.

Apart from the Adriatic Sea, the region is the second deep-water formation zone within the Mediterranean basin, with its main source areas reported to be the North Aegean continental shelf and the eastern Cretan margin [74–76]. The Black Sea freshwater discharges during cold atmospheric fronts in the winter determine the magnitude of dense deep-water supply [77], while the Cretan Gyre (including its peripheries to the east up to Rhodes Island) in the south Aegean further functions as a source of both intermediate and deep waters [76,78], and, therefore, can be considered to be the main contributor in triggering changes in the eastern Mediterranean thermohaline circulation (Eastern Mediterranean Transient; [75]).

3. Material and Methods

3.1. Study Core

The 2.8 m length gravity core NS-18 used in this study was retrieved during the 1998 R/V Aegaeo cruise from 496 m water depth at the easternmost edge of the recent Aegean volcanic arc (36°31.32' N, 27°16.15' E) in the south Aegean Sea. NS-18 core contains distinct organic-rich dark interval representing the regional expression of sapropel S1 [79], and comprises the last ~20 ka. The lower part of the core, below 230 cm, consists of olive-gray coarse sands of turbiditic origin, and, therefore, was excluded from further analyses. For the detailed description of the core lithology, we referred to Triantaphyllou [80].

3.2. Radiocarbon Analyses

Four accelerator mass spectroscopy (AMS) ¹⁴C measurements were performed on hand-picked mixed *Globigerinoides ruber* and *Globigerinoides trilobus* specimens in the size fraction >125 μm. It is worthy to note that the selected samples were related to abundance peaks to minimize the effect of bioturbation. The datings at 57 and 255 cm were performed at Beta Analytics laboratories at Miami, Florida (USA) in 2009, and those at 159 and 201 cm at the University of California, Irvine in 2022 (Table 1). Conventional radiocarbon datings were corrected using the regional marine reservoir correction of 58 ± 85 years [81], and then calibrated to calendar years using the INTCAL20 calibration curve in the Calib 8.2 software [82].

Table 1. Accelerator mass spectroscopy (AMS) ¹⁴C datings for the core NS-18.

Core Depth (cm)	AMS Lab Code	Conventional ¹⁴ C Age (yr)	Calibrated Age (yr cal BP)	2σ Age Range
56–58	Beta-253709	4690 ± 40	4710	4570–4850
158–160	UCIAMS-256864	11,020 ± 25	11,020	11,956–12,572
200–202	UCIAMS-256865	14,350 ± 35	16,472	16,144–16,800
254–256	Beta-303651	18,300 ± 80	21,260	21,110–21,410

3.3. Micropaleontological Analyses

The planktonic foraminiferal assemblages identified in the 49 downcore sediments were picked from ~10 cm³ of wet sediment after washing through a 125 μm mesh sieve and cleaning using the HyPerCal protocol [83]. Following the findings of Capotondi et al. [84], particularly for the study area, the adopted size fraction provides a more realistic spectrum of the planktonic foraminiferal assemblage in the Mediterranean Sea. The dry residues (~3 g) were split using an Otto micro-splitter into aliquots of at least 300 planktonic foraminiferal specimens, thus providing a significant level of at least 95% for species of greater than 3% relative abundance [85]. After identification to species level based on Hemleben et al. [86] and Brummer and Kučera [87], they were sorted on Chapman slides and counted. Raw data were transformed into percentages of the total absolute abundance, and relative percentage abundance curves of the most representative species were plotted versus core depth in Grapher. For detailed species-specific morphological recognition and micropaleontological groupings among the studied species, we refer to the studies of Kontakiotis et al. [17], and, for the subsequent ecological interpretations, we refer to those of

Zarkogiannis et al. [16], Kontakiotis et al. [28], Giamali et al. [19], and Kozanoglou et al. [88], particularly for the Mediterranean Sea.

4. Results

4.1. Planktonic Foraminiferal Assemblages

A qualitative analysis of planktonic foraminifera allows us to identify 20 species lumped into 14 groups: *Globigerinoides ruber alba*, *Globigerinoides ruber rosea*, *Globigerinoides trilobus* gr., *Globigerinoides bulloides* gr., *Globigerinella siphonifera* gr., *Orbulina universa*, *Globoturborotalita rubescens* gr., *Globoturborotalita glutinata*, *Globorotalia scitula*, *Globorotalia inflata*, *Neogloboquadrina pachyderma*, *Neogloboquadrina dutertrei*, *Globorotalia truncatulinoides*, and *Turborotalita quinqueloba*. Their relative abundances (%) versus core depth are displayed in Figure 2. Along the study interval, assemblages are mainly represented by *G. ruber* (*alba* and *rosea*) and *G. bulloides*. The former is the most abundant species, especially in the south Aegean with percentages of up to 50%, and, together with the latter, represent about 80% of the entire population. The remaining species are composed mostly of the surface- and subsurface-dwelling species (*G. trilobus*, *G. rubescens*, *O. universa*, and *G. siphonifera*) corresponding to the SPRUDTS group [89], with average percentages of ~10%, while deeper-dwellers and cold-water species (e.g., *G. scitula*, *G. inflata*, and *T. quinqueloba*) appear with lower percentages. Both representatives of Neogloboquadriniids (*N. pachyderma* and *N. dutertrei*) present a sporadic distribution since they are significant contributors only in the lower part of the core with an average contribution of ~30–40%.

4.2. Bioevent Stratigraphy

The observed planktonic foraminiferal abundance fluctuations are consistent with previously documented changes in the study area, the comparison of which allows us to define a series of biochronological events. Each event is defined by sharp frequency shifts or by local occurrence/disappearance alternations of the identified species. The advantage of the combination of these bioevents with the most complete (combining planktonic foraminifera, coccolithophores, and pollen) eco-biozonation scheme of Triantaphyllou et al. [3] for the Aegean Sea, established for the well-dated core NS-14 (near to NS-18), offers a stratigraphically controlled and more high-resolution subdivision of the Late Pleistocene–Holocene. Overall, we identified, described, and dated up to 30 bioevents (Figure 2), of which 10 are Mediterranean-wide synchronous (symbolized with “s”) and 20 (those of Pérez-Folgado et al. [48] enriched with the newly defined) are diachronous (symbolized with “d”). In the case of the Pérez-Folgado et al. [48] bioevents, we kept the nomenclature introduced by these authors by also determining their timing ranges, in which certain species reach values well above or below their average percentages. The earlier or delayed event among different Mediterranean sub-basins could be mostly attributed to species-specific ecological preferences in conjunction with relevant hydrographic parameters and oceanic circulation. In addition, the identification of the described bioevents in other more or less distant cores permits precise intra- and inter-basinal correlations and facilitates regional palaeoceanographic interpretations for the studied time interval.

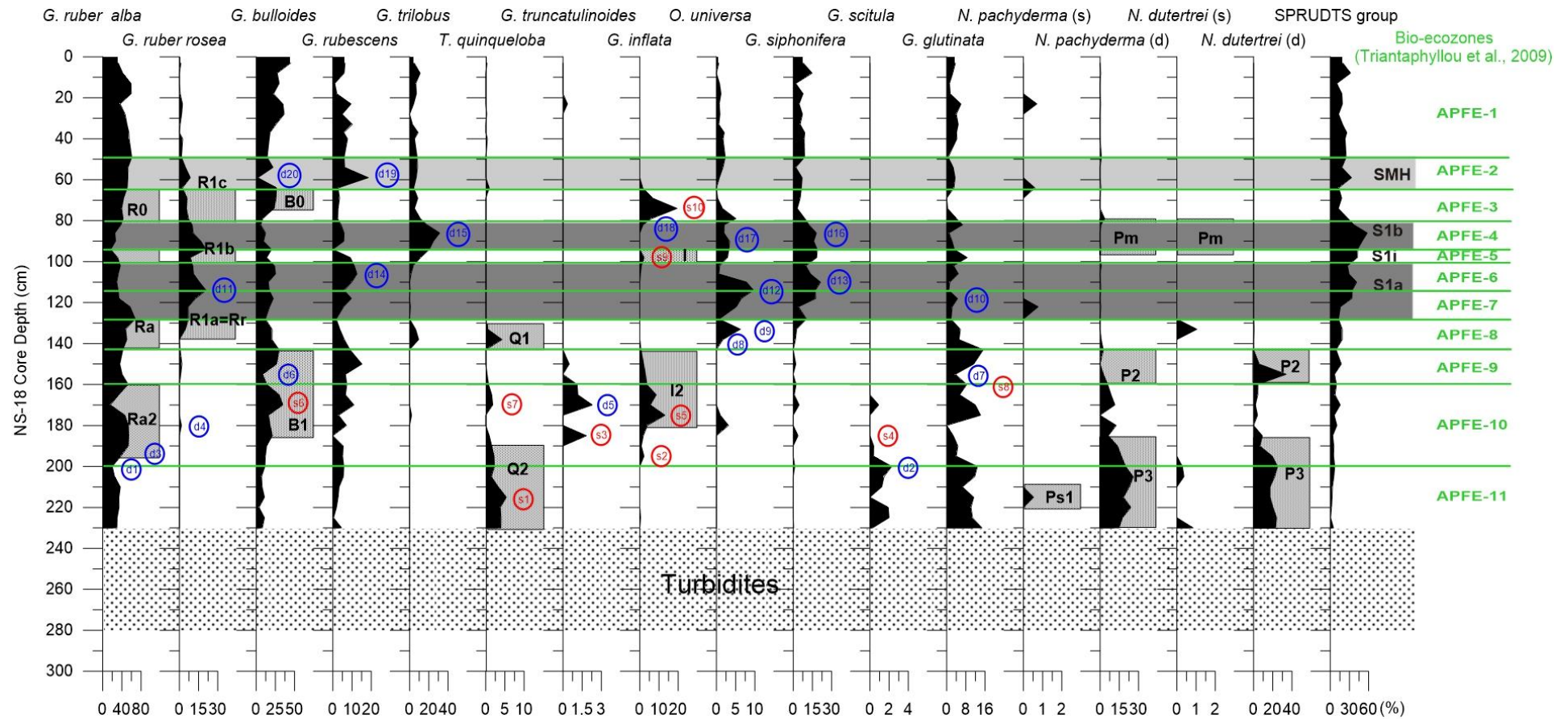


Figure 2. Frequency curves and recognized bioevents (synchronous in red and diachronous in blue) of the most representative planktonic foraminiferal species in core NS-18. To the right, the established Aegean bio-ecozones of Triantaphyllou et al. [3] are presented in green. Dark grey bands correlate to sapropel S1 depositional intervals, while the light grey one to the equivalent to the Sapropel Mid Holocene (SMH) [90] layer.

5. Discussion

5.1. High-Resolution Mediterranean Bio-Ecochronological Events Deduced from Planktonic Foraminiferal Assemblages

In biochronological studies, bioevents are often identified on entries, exits, and significant shifts in the faunal record [44], usually displayed by species-specific relative abundances. Moreover, frequency shifts illustrated in relative abundance plots reflect population shifts rather than evolutionary changes among species. Especially in marginal basins like the Aegean Sea, the successive planktonic foraminiferal zones can be indicated as bio-ecozones, because most of the species are sensitive indicators of past environmental changes with amplified signals [45]. Therefore, the integrated concept of “assemblage bio-ecozones” supplemented with the “species-specific planktonic foraminiferal bioevents” adopted here refers to their response to environmental changes in specific time intervals. The synchronous or diachronous nature of these bioevents could be further considered as Mediterranean-basin-wide or only local (or even an asynchronous expression), depending on their occurrence.

5.2. Planktonic Foraminifera Fluctuations along the Mediterranean Basin: Calibrating the Synchronous Bioevents

The comparison of NS-18 planktonic foraminiferal distribution patterns with those reported from deep-sea cores from eastern (e.g., NS-14, C69, C40, SK-1, SL-11, SL-21, SL-31, SLA-9, LC-21, ST5, and MD84-641; [3,6,44,46,88]) and western (e.g., MD95-2043; ODP 977, REC13-53, KET80-19, Hole 963D, BS79-22, BS79-38, and GNS84-C106; [48,51–54]) basins displayed some Mediterranean-wide assemblage fluctuations over the glacial–interglacial timescale. At the regional scale, these trends could be considered quite synchronous, considering the 2σ uncertainty, even though minor dating differences (possibly related to the available radiocarbon datasets and uncertainties in the different age models) exist.

Based on the existing, well-documented records across the Mediterranean Sea, a mean age of each recognized bioevent was determined, and then intercalibrated through the comparison with the planktonic foraminiferal bioevents and related bio-ecozonation derived from the nearby well-dated core NS-14 [3]. The sequence of the resulting ages (Table 2) in the core NS-18 stratigraphy revealed an excellent match with AMS datings and, therefore, manifests that these events are well-constrained temporally in the eastern Mediterranean, also reflecting the accuracy of the adopted chronostratigraphic approach.

Table 2. Mediterranean-wide synchronous age model pointers, derived from the study core NS-18 and calibrated with other available Mediterranean reference records. Sapropel S1 and SMH layers control points are also added.

Synchronous Planktonic Foraminiferal Bioevents within the Mediterranean Sea	Control Points	AMS ¹⁴ C	Depth (cm)	Age (ka cal BP)
(s1) Last glacial peak of <i>T. quinqueloba</i>			215	18.3
		AMS	201	16.47
(s2) First post-glacial occurrence of <i>G. inflata</i>			195	15.3
(s3-s4) Last post-glacial occurrence of <i>G. truncatulinoides</i> and disappearance of <i>G. scitula</i>			185	14.5
(s5) <i>G. inflata</i> maximum abundance during B/A			175	13.5
(s6-s7) <i>T. quinqueloba</i> and <i>G. bulloides</i> peaks during YD			170	12.8
(s8) <i>G. glutinata</i> peak at the B/A-YD boundary			160	12.3
		AMS	159	12.26
(s9) Frequency increase of <i>G. inflata</i> during the sapropel interruption S1i	Base S1a		128	10
	Top S1a		102	7.9
			98	7.7
(s10) <i>G. inflata</i> peak after the end of sapropel S1	Base S1b		94	7.3
	Top S1b		82	6.4
			74	5.8
(s10) <i>G. inflata</i> peak after the end of sapropel S1	Base SMH		64	5.4
		AMS	57	4.71
	Top SMH		49	4.3

Over the last ~20 kyr, we identified ten bioevents that can be further used as control-points to define or strengthen the chronology of Mediterranean marine sediment cores. Most of them correspond to the termination T1, while one is reported for the latest Glacial and two for the Holocene (Table 2).

During the latest Glacial period, the last increase of *T. quinqueloba* (bioevent s1) dated at 18.3 ka is marked. This *T. quinqueloba* spike close to the end of the Last Glacial Maximum (LGM) has also been observed in several records across the Mediterranean Sea from the Alboran (bioevent Q2 at 18.3 ka [48]) to the Tyrrhenian basin (18.2 ka [52]; ~18 ka [54]), and through the Siculo-Tunisian Strait (18.3 ka [91,92]) up to the Levantine Sea (18.3 ka [46]).

Seven distinct and quite synchronous bioevents characterize the deglaciation period. The first post-glacial occurrences of *G. inflata* and *G. truncatulinoides* (bioevents s2 and s3) are recorded at 15.3 and 14.6 ka, respectively [46]. The post-glacial reappearance of *G. inflata* during the Bølling–Allerød (B/A) has been dated at 15.3 ka in Hole 963D [51] and core Z1 [63], at 15.4 ka in MD90-917 [61], at 15.1–15.2 ka in cores BS79-22 and BS79-38 [52,53], and at 15.6 ka in core MD84-641 [46] in the Levantine Sea. The first post-glacial occurrence of *G. truncatulinoides* was dated at 14.5 ka in the Levantine Sea (core MD84-641 [46]) and the south Adriatic Sea (core MD90-917 [61]), in accordance with other records from the central Adriatic (core CM92-43 [59,60]) and Tyrrhenian Sea (core KET80-19 [46]). The time equivalent with the reoccurrence of *G. truncatulinoides* is the last common postglacial disappearance of *G. scitula* (bioevent s4), which has also been dated at around 14.5 ka within the Mediterranean basin [7,46,63]. The existing dating discrepancies in the literature regarding this bioevent cannot be considered as a significant offset, since, in some cases, it is described as an abundance decline (at 14.8 ka in core REC13-53 and at 14.3 ka in core KET80-19; [46]), while, in others, as the last occurrence of this subpolar species (at 13.9 ka core MD90-917; [61] or ~14.0 ka in cores MD04-2797 and MD 04-2797 CQ; [91,92]; core BS79-38; [53,54]; core KIM-2A; [5]; and core SK-1; [9,93]). In all locations, this bioevent reflects the base of Marine Isotope Stage 1 [92,94], and, consequently, the climate amelioration during the B/A warm period in the entire Mediterranean basin [4,8,9,61,63]. The next bioevent corresponds to an increase in the abundance of *G. inflata* during that period (bioevent s5), characterized by two consecutive peaks, the highest of which has been dated at 13.5 ka [59]. Compared to other Mediterranean sites, the relatively lower percentages of this deep-dwelling species recorded here could be attributed to the lower bathymetry of the NS-18 core site (496 m water depth). This shallow depth site probably prevents the occurrence of deep-dwelling species such as *G. scitula*, *G. truncatulinoides*, and *G. inflata*, favoring, in parallel, the increased abundance of the surface-dwelling species (e.g., *G. ruber*).

At 12.8 ka, the assemblage is punctuated by the simultaneous peaks of *G. bulloides* and *T. quinqueloba* (bioevents s6 and s7). Similarly with other planktonic records across the Mediterranean Sea [3,46,51,54], these bioevents were accompanied by a decline in *G. ruber* (w). The Aegean records (e.g., NS-18 and NS-14) show a remarkable resemblance with those from the central Mediterranean (e.g., REC13-53, KET80-19, and GNS84-C106), with only some slightly discrepancies to be observed on the related taxa abundances, which could be attributed to the different mesh sieves used in these studies that essentially led to the loss of the small-sized species such as *T. quinqueloba* and, consequently, increased percentages of *G. ruber* (w). However, the high occurrence of the *G. ruber* taxon living in warm surface waters reflects the SST increase in the studied area. The end of the B/A and the onset of the Younger Dryas (YD) period was marked by two coeval peaks of *G. ruber* (w) (53%) and *G. glutinata* (9%; bioevent s8) at 12.3 ka. Similar bioevents have been also recognized in several basins along the Mediterranean basin (e.g., Sicily Channel—ODP Leg 160, Site 963; [51], Tyrrhenian Sea—GNS84-C106, KET80-19, BS79-22, BS79-38; [52,53], Aegean cores of [44], MNB3; [8]; MD84-641; [46]). The age of 12.26 ka derived from an AMS analysis in NS-18 (159 cm depth) fully supports the synchronicity of this bioevent into the Mediterranean basin. According to Casford et al. [95], the peak of *G. glutinata* (up to 15% in NS-18) within the YD reflects the Termination T1b onset.

During the Holocene, the maximum abundances of *G. inflata* during the interruption (3% at 7.7 ka; bioevent s9) and after the end (20% at 5.8 ka; bioevent s10) of sapropel S1 are synchronous along the central-eastern Mediterranean Basin. The former (at 7.7 ka bioevent I; [48]) has also been recognized in the western Mediterranean, while the latter, particularly, has been interpreted as the re-establishment of deep-water ventilation in the eastern Mediterranean [3,6,9]. Both the bioevents have been documented in numerous central and eastern Mediterranean cores [3–8,19,44,46,52,61,63,95–97], and interpreted as the results of the intensification of vertical mixing during a cold event [4].

5.3. Integrated Age Model

The integrated chronostratigraphy of the core NS-18 is based on four AMS ¹⁴C dates, and on the additional control points which correspond to well-dated lithostratigraphic levels (e.g., sapropel S1 and SMH boundaries) within the eastern Mediterranean basin (Table 2, Figure 3). Although the SMH is not lithologically evident in the study core, the similar faunal signals derived from NS-18 (Figure 2) and the reference NS-14 core [3] indicate that it can be used as an additional stratigraphic point, particularly for that sub-basin.

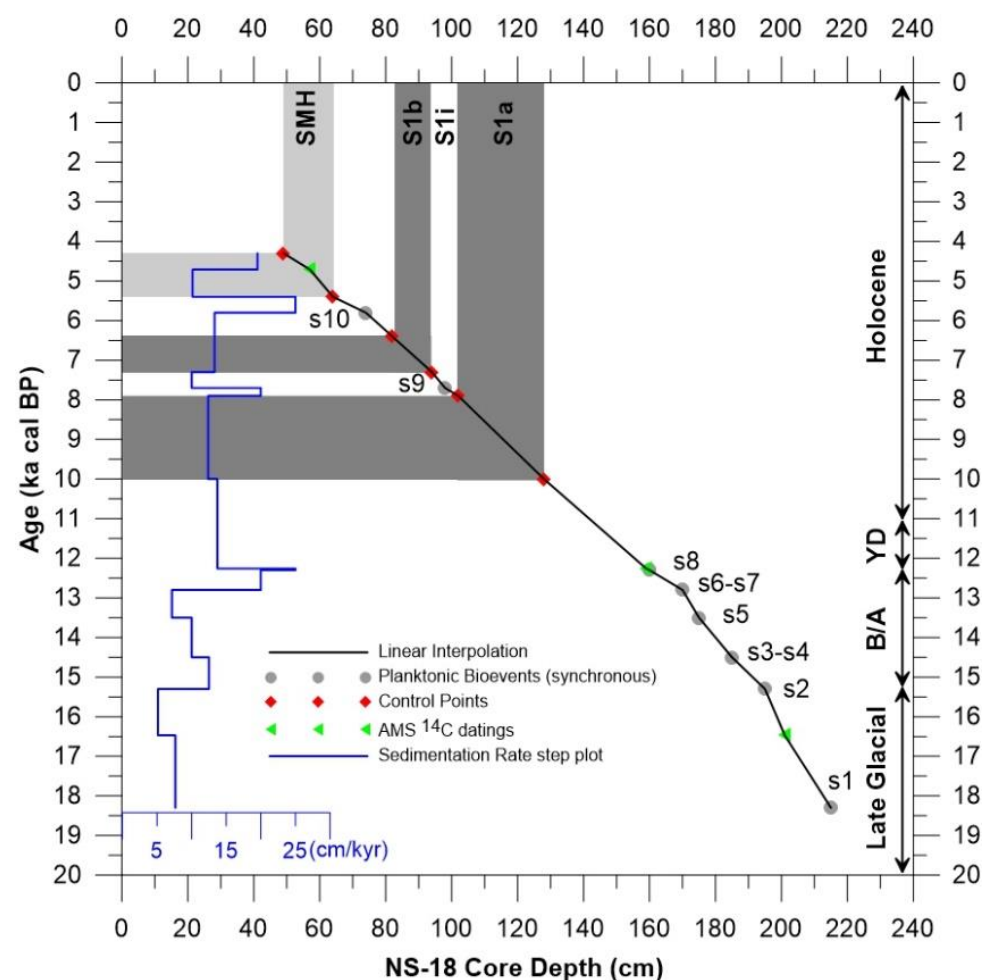


Figure 3. Integrated age model (black line), using the calibrated ages of the Mediterranean-wide synchronous planktonic bioevents (s1–s10, grey circles; Table 2), the available AMS datings (green triangles; Table 1), and sapropel layer control points (red diamonds; Table 2), along with the derived sedimentation rates (blue line) of the core NS-18. Dark grey bands correlate to sapropel S1 depositional intervals, while the light grey one corresponds to the equivalent to the SMH interval [90].

Furthermore, the calibrated planktonic foraminiferal bioevents described above as Mediterranean-wide synchronous (Table 2) have been integrated in the NS-18 age model

as additional dating points allowing for a high-resolution chronostratigraphic framework covering the last ~20 kyr. The resulting age model was constructed by linear interpolation between all the above dating points as shown in Figure 3. We note that the AMS dating at 255 cm, although it seems reliable (21.26 ka cal BP; Table 1), was not used in the age model construction because the entire interval below 230 cm consists of sands, interpreted as being of turbiditic origin linked to the rapid sea level rise during the early stages of the last deglaciation [3,33,90] or associated with seismically induced landslide events [98]. Nevertheless, we consider the analyzed sedimentary succession (0–230 cm) above this event as continuous, which is further supported by the fact that equivalent bio-ecozones and the relevant bioevents were recognized in several basins within the entire Mediterranean Sea.

5.4. Diachronous Bioevents for Improving Local Aegean Biostratigraphic Schemes and Their Paleooceanographic Implications

In a regional context, the Aegean Sea represents an ideal basin to develop an integrated biochronological framework owing to exceptionally high accumulation rates and enhanced paleoceanographic information derived from the high-resolution planktonic foraminiferal records throughout the basin since the last glacial–interglacial transition [3–9,19,88]. Hence, supplementary to the known bioevents of Pérez-Folgado et al. [48], we identified 20 additional bioevents expressed locally in the Aegean Sea (Table 3).

Table 3. Newly defined diachronous planktonic bioevents for the Aegean Sea, derived from the integrated NS-18 age model.

Newly Defined Diachronous Planktonic Bioevents in Aegean Sea	Depth (cm)	Age (ka cal BP)
(d1) Decrease of <i>G. ruber</i> (w) at the end of the Latest Glacial	200	16.2
(d2) Increase of <i>G. scitula</i> during the Oldest Dryas	200	16.2
(d3) Increase of <i>G. ruber</i> (w) at the start of Bølling–Allerød (base of bioevent Ra2)	190	14.9
(d4) First occurrence of <i>G. ruber rosea</i> during the deglaciation	180	14.0
(d5) <i>G. truncatulinoides</i> maximum during the Bølling–Allerød	170	12.8
(d6) Minimum abundance of <i>G. bulloides</i> during the Younger Dryas	155	11.97
(d7) Minimum abundance of <i>G. glutinata</i> during the Younger Dryas	155	11.97
(d8) Re-occurrence of <i>O. universa</i> with the start of Holocene	138	10.73
(d9) Maximum abundance of <i>O. universa</i> below the sapropel S1	133	10.36
(d10) Peak in abundance of <i>G. glutinata</i> within S1a	118	9.2
(d11) Peak in abundance of <i>G. ruber rosea</i> within S1a	114	8.87
(d12) Peak in abundance of <i>O. universa</i> within S1a	114	8.87
(d13) Maximum abundance of <i>G. siphonifera</i> within S1a	110	8.55
(d14) <i>G. rubescens</i> peak within S1a	106	8.23
(d15) <i>G. trilobus</i> peak within S1b	86	6.7
(d16) <i>G. siphonifera</i> peak within s1b	86	6.7
(d17) <i>O. universa</i> peak within s1b	90	7.0
(d18) Near absence of <i>G. inflata</i> at the top of S1b	82	6.40
(d19) <i>G. rubescens</i> peak within SMH	59	4.91
(d20) <i>G. bulloides</i> decline during SMH (top of bioevent B0)	59	4.91

Due to the turbidites' presence at the base of the core NS-18, only the uppermost part of the Late Glacial period, including the LGM, is present and is ascribed to the bioecozone APFE-11 [3]. The most pronounced faunal fluctuation recovered during this timespan is the peak in the abundance of Neogloboquadriniids (bioevent P3; [48]). The maximum in the abundance of both the deep-dwelling representatives *N. pachyderma* (dex) and *N. dutertrei* (dex) of this group is indicative of cold and productive waters associated with a well-developed Deep Chlorophyll Maximum (DCM) at the base of the euphotic layer [96,99,100]. The particularity of the LGM in the Aegean Sea is the mixture between cold (*G. scitula*, *T. quinqueloba*, *N. pachyderma*, *N. dutertrei*, and *G. glutinata*)- and warm (*G. ruber* (w) and *G. rubescens*)-water species. Despite the dominance of cold-water species during that time, noticeable percentages (up to ~40%) of *G. ruber* (w) were observed in the Aegean in accordance with other sub-basins (e.g., Adriatic, Tyrrhenian, and

Alboran; [3,61,101–103]), probably reflecting a slight SST rise. A sharp decrease (in the half ~20%; bioevent d1) of *G. ruber* at 16.2 ka marks the end of the LGM, which is also coeval with the upper boundary of this biozone. Consistent with previous records from the central Mediterranean, the simultaneous increase of *G. scitula* (bioevent d2) characterizes the Oldest Dryas climatic event and possibly reflects a decrease in salinity [61,91,104]. In the north Aegean, this enhanced faunal proportion of *G. scitula* has been recorded with two distinct peaks at 17.0 and 15.8 ka [8], while, in the Adriatic, it has been traced at 16.9 ka [61] respectively.

The interval covered by the bio-ecozone APFE-10 corresponds to the first climatic phase of the last deglaciation in terms of the interstadial Bølling–Allerød dated between ~15.0 and 13 ka in the Aegean Sea. A slight increase in the planktonic foraminiferal diversity characterizes this interval dominated by warm-to-temperate species (e.g., *G. ruber* (w), *G. inflata*, *G. bulloides*, *N. pachyderma*, and *G. glutinata*). The onset of the Bølling in the NS-18 core is dated at 14.9 ka, comparable to the Greenland ice core records (14.69 ka), as well as other records within the entire Mediterranean [5,8,55,61], and is characterized mostly by the sudden increase of *G. ruber* (w) (bioevent d3 at the base of bioevent Ra2 at 14.8 ka; [48]) reflecting the climatic amelioration. The increased contribution of this species in the fauna, which almost reached Holocene values, was accompanied by the first occurrence of *G. ruber rosea* at 14.0 ka (bioevent d4), the re-entry of the warm indicators *G. siphonifera* and *O. universa*, and a significant decrease of *G. scitula* and *T. quinqueloba*. The *G. glutinata* shift displayed by maximum percentages of 14% is recorded contemporaneously with the major peak of *G. inflata* (bioevent I2; [48]) at 13.5 ka. These bioevents, together with the *G. truncatulinoides* peak at 12.8 ka (bioevent d5), suggest strong vertical mixing within a relatively cool, mesotrophic water column in the south Aegean Sea. The productivity increase during that time is further supported by the significant rise in *G. bulloides* (bioevent B1; [48]), culminating in a peak (35%) at 12.8 ka.

The bio-ecozone APFE-10 between 12.3–11.6 ka corresponds to the Younger Dryas cooling event revealed by the increase in cool-water and decrease in warm-water species, respectively. The significant contribution of *G. bulloides*, and *N. dutertrei* suggest a strengthening of winter convection and strong marine eutrophication, which is further supported by the noticeable occurrence of *G. glutinata*, an opportunistic species to nutrient availability. Moreover, the progressive reduction in *G. inflata* and *G. truncatulinoides* and the increase in Neogloboquadriniids (also evident in the Sicily Channel; [51]) further imply that seasonal water column homogenization favored during the B/A became inhibited during that period. The minimum concentrations of *G. bulloides* (bioevent d6) and *G. glutinata* (bioevent d7) at 11.97 ka may indicate mild climate conditions in the middle of the YD, reinforcing the findings about distinct climate phases (two cold phases at the top and the base and a third warm in between, based on terrestrial proxies, in contrast to a more weakened signal with two phases in the marine microfauna records) identified both locally within the Mediterranean basin [8,9,105–107] and globally [108–110].

This stadial environment appears to alter at 11.6 ka, representing a transitory phase at the beginning of the Holocene until the onset of the sapropel deposition. The abrupt switch to warmer conditions is marked by the near-disappearance of all cold water indicators and the abrupt increase in warm-water species belonging to the SPRUDTS group. This regime in the Aegean Sea is also characterized by the re-occurrence of *O. universa* at 10.73 ka (bioevent d8), a species which progressively increases its abundance from its lowest values recorded at 10.48 ka [88] and reaches a maximum abundance at 10.36 ka (bioevent d9), as well as the turnover between *G. inflata* and *G. glutinata* which has been interpreted in terms of seasonality [9,95]. The increased percentages of *T. quinqueloba* at 10.73 ka (bioevent Q1; [48]) could be associated with the brief cooling event centered at around 10.5 ka [4,8] and the drop in the warm/cold plot below the sapropel at 10.48 ka [44,88].

By 10.0 ka, the onset of the sapropel deposition represents the Holocene Climatic Optimum testified mostly by the acme interval of both chromotypes of *G. ruber* (bioevents Ra and R1a; [48]) in the planktonic fauna. However, the detailed planktonic foraminiferal

record throughout both sapropel units (S1a and S1b), including the interruption (S1i), allows the identification of several bioevents indicative of the changing environmental conditions, particularly for that marginal basin. Generally, the fauna shows an abrupt increase in warm mixed layer species and the near absence of cold-water species, reflecting a pronounced warming of surface waters that is also portrayed in the Aegean SST records [90,111]. A remarkable feature of the planktonic foraminiferal assemblages is also the distinctive decrease in Neogloboquadriniids within the sapropel, previously recognized as the bioevent Pm [48]. At the base of the bio-ecozone APFE-7 corresponding to the lower part of S1a, a rise in *G. glutinata* is recorded at 9.2 ka (bioevent d10). Considering the cosmopolitan character of this species together with similar reports from the south Adriatic basin at around 9.0 ka [96], the *G. glutinata* spike could possibly reflect enhanced primary productivity with the sapropel onset in the southeastern Mediterranean. Such an interpretation is further supported by elevated Ba/Al values measured in many cores retrieved from the Aegean and Adriatic sub-basins [4,44,79,90,112]. The top of S1a (eco-biozone APFE-6; [3]) is characterized by the increase in warm oligotrophic species, as evidenced by the relevant spikes (in order from the oldest to the newest) of *G. ruber rosea*, *G. siphonifera*, *O. universa*, and *G. rubescens*. Among the above representative species, *G. ruber rosea* (bioevent d11) and *O. universa* (bioevent d12) present a peak at the onset of the bio-ecozone APFE-6 (8.87 ka), followed by the *G. siphonifera* maximum abundance dated at 8.55 ka (bioevent d13), and an increasing trend of *G. rubescens* centered at 8.23 ka (bioevent d14). The progressive increase in abundance observed for all these members of the SPRUDTS group is indicative of an increase in the depth and extent of the thermocline during the deposition of S1a.

Within the brief interval of the bio-ecozone APFE-5, a significant turnover was documented in the planktonic fauna reflected by the decline in all warm water species and the increase in cold-water species (e.g., *G. glutinata* and *G. inflata*), respectively. The re-occurrence of *G. inflata* during the sapropel interruption S1i was the result of temporary stronger water column ventilation, probably triggered by cold and dry conditions (8.2 kyr event; [113]), as evidenced all over the Mediterranean basin [1,4,8,51,114–116]. Vigorous vertical mixing of a relatively cool water column enriched in nutrients is testified by the *G. inflata* peak (bioevent I; [48]). The mixing was intense to prevent water mass stratification during S1i in the south Aegean Sea. However, the NS-18 record shows that these conditions did not prevail for a long time. The multi-centennial climate deterioration was accompanied by warm climate conditions reflected by the increase in warm indicators during the deposition of S1b (eco-biozone APFE4; [3]). The considerable increase in the SPRUDTS group reflected mostly by peaks of *G. trilobus* (bioevent d15) and *G. siphonifera* (bioevent d16) at 6.7 ka and, subordinately, of *O. universa* (bioevent d17) indicate a shallow pycnocline. The near absence of *G. inflata* within S1b (particularly at the top; bioevent d18), compared to its previous peak during the S1i, hints that reduced oxygenation in the deep-water column was detrimental to this species, suggesting the persistent lack of winter mixing in a quite stratified (poorly ventilated) water column (supported also by the absence of oxic benthic species). In accordance with similar records along the Aegean Sea, its last entrance in the top of S1b was dated at 6.4 ka [44] or 6.87 ka [88].

After the termination of the sapropel S1 deposition (bio-ecozone APFE-3), *G. inflata* registers another peak (bioevent s10 at 5.8 ka) before its local disappearance at 5.51 ka [88], which has been ascribed to an overturning reinforcement and reventilating of the Aegean deep waters [117]. Despite the predominance of *G. ruber* (bioevent R0; [48]), the rise in the abundance of *G. bulloides* (bioevent B0; [48]) might be explained by phytoplankton blooms induced by enhanced nutrient availability in shallow waters. During the eco-biozone APFE-2, the local deposition of SMH in the south Aegean of between 5.4 and 4.3 ka is the most pronounced environmental perturbation, pinpointed by the sapropel-like fauna. *G. ruber alba* (bioevent R0; [48]) and *G. ruber rosea* (bioevent R1c; [48]) are the dominant species, while a significant rise in *G. rubescens* is also observed at 4.91 ka (bioevent d19). Interestingly, the *G. bulloides* decline (bioevent d20) is marked at the same time, culminating in the bioevent B0. The NS-18 core recorded significant percentages of *G. bulloides* and

G. trilobus, indicating fresher (sub)surface waters. Overall, the regime of that warm and humid phase is characterized by the strengthening of the summer stratification [80]. Finally, the bio-ecozone APFE-1 is dominated by the *G. ruber alba*, *G. rubescens*, *G. siphonifera*, and *G. glutinata* assemblage which is consistent with the salinity increase and oligotrophic and dry nature of the water column of the modern Aegean Sea [9,16].

6. Conclusions

We performed here a detailed micropaleontological study to generate accurate biochronological events, considered to be the key requirements for a precise age model construction. The high-resolution micropaleontological study performed on the core NS-18 from the south Aegean Sea provides a continuous record of faunal changes over the last 20 ka, reflected mostly by turnovers and abundance variations in the planktonic fauna during the Late-Glacial-to-Holocene transition. Major changes in the planktonic foraminiferal record, reflected mostly by deglacial appearance/disappearance alterations, display synchronous patterns along the different Mediterranean sub-basins, and, therefore, such bioevents can be used for the establishment of the core chronology. Moreover, downcore variations in the abundance distributional patterns of the most representative species represent additional diachronous bioevents that can be used to refine or extend previous local eastern Mediterranean biostratigraphic schemes. These results, integrated with the existing Aegean bioecozonation, are also consistent with the most important Late-Glacial-to-Holocene paleoclimatic (e.g., Bølling–Allerød, Younger Dryas) and paleoceanographic (e.g., S1 and SMH deposition) events in the eastern Mediterranean, facilitating regional climatic and/or microfaunal correlations. The correlation between the planktonic stratigraphic distribution and paleoclimatic/paleoceanographic conditions expressed by the species-specific ecological preferences further reveal the high potential of this multi-disciplinary approach in stratigraphic, paleoclimatic, and paleoecological studies. However, we emphasize that additional records covering all intra-Mediterranean sub-basins are required to ensure the applicability of this multi-disciplinary proxy.

Author Contributions: Conceptualization, G.K. and A.A.; methodology, G.K., A.A. and M.V.T.; software, G.K.; validation, G.K., A.A., E.B., E.S. and M.V.T.; formal analysis, G.K.; investigation, G.K., A.A., E.B., E.S. and M.V.T.; resources, M.V.T.; data curation, G.K., A.A. and M.V.T.; writing—original draft preparation, G.K.; writing—review and editing, G.K., A.A., E.B., E.S. and M.V.T.; visualization, G.K., A.A. and M.V.T.; supervision, A.A. and M.V.T.; project administration, G.K., A.A. and M.V.T.; funding acquisition, G.K. and M.V.T. All authors have read and agreed to the published version of the manuscript.

Funding: This research received no external funding.

Institutional Review Board Statement: Not applicable.

Informed Consent Statement: Not applicable.

Data Availability Statement: The data used in this work are available upon request from the corresponding author.

Acknowledgments: The APC of this article has been funded by the National and Kapodistrian University of Athens (KE 19432); Internationalization of Higher Education actions MIS 5164455.

Conflicts of Interest: The authors declare no conflict of interest.

Appendix A

Label in Figure 1	Core Name	Reference
1	MD84-641	[46]
2	LC-31	[44]
3	NS-18	This study
4	NS-14	[3,90]

Label in Figure 1	Core Name	Reference
5	LC-21	[44]
6	KIM-2A	[5]
7	C69	[6]
8	C40	[7,44]
9	SL-9	[44]
10	SL-11	[44]
11	SL-21	[44]
12	SL-31	[44]
13	SK-1	[9,44]
14	MNB-3	[111]
15	AEX-15	[4,19]
16	AEX-23	[4]
17	M4-G	[118]
18	SL-152	[119,120]
19	Z1	[63]
20	MD90-917	[61]
21	IN68-9	[44,57]
22	CM92-43	[59,60]
23	GNS84-C106	[54]
24	KET80-19	[46]
25	BS79-22	[52]
26	BS79-38	[53]
27	ODP SITE-963	[51]
28	REC13-53	[46]
29	Hole 963 D	[51]
30	MD95-2043	[48]
31	ODP977	[48]
32	ST5	[88]

References

- Marino, G.; Rohling, E.J.; Sangiorgi, F.; Hayes, A.; Casford, J.L.; Lotter, A.F.; Kucera, M.; Brinkhuis, H. Early and middle Holocene in the Aegean Sea: Interplay between high and low latitude climate variability. *Quat. Sci. Rev.* **2009**, *28*, 3246–3262. [\[CrossRef\]](#)
- Rohling, E.J.; Marino, G.; Grant, K.M. Mediterranean climate and oceanography, and the periodic development of anoxic events (sapropels). *Earth-Sci. Rev.* **2015**, *143*, 62–97. [\[CrossRef\]](#)
- Triantaphyllou, M.V.; Antonarakou, A.; Kouli, K.; Dimiza, M.; Kontakiotis, G.; Papanikolaou, M.D.; Ziveri, P.; Mortyn, P.G.; Lianou, V.; Lykousis, V.; et al. Late Glacial–Holocene ecostratigraphy of the south-eastern Aegean Sea, based on plankton and pollen assemblages. *Geo-Mar. Lett.* **2009**, *29*, 249–267. [\[CrossRef\]](#)
- Giamali, C.; Koskeridou, E.; Antonarakou, A.; Ioakim, C.; Kontakiotis, G.; Karageorgis, A.P.; Roussakis, G.; Karakitsios, V. Multiproxy ecosystem response of abrupt Holocene climatic changes in the northeastern Mediterranean sedimentary archive and hydrologic regime. *Quat. Res.* **2019**, *92*, 665–685. [\[CrossRef\]](#)
- Giamali, C.; Kontakiotis, G.; Koskeridou, E.; Ioakim, C.; Antonarakou, A. Key Environmental Factors Controlling Planktonic Foraminiferal and Pteropod Community’s Response to Late Quaternary Hydroclimate Changes in the South Aegean Sea (Eastern Mediterranean). *J. Mar. Sci. Eng.* **2020**, *8*, 709. [\[CrossRef\]](#)
- Geraga, M.; Tsaila-Monopolis, S.; Ioakim, C.; Papatheodorou, G.; Ferentinos, G. Short-term climate changes in the southern Aegean Sea over the last 48,000 years. *Palaeogeogr. Palaeoclimatol. Palaeoecol.* **2005**, *220*, 311–332. [\[CrossRef\]](#)
- Geraga, M.; Tsaila-Monopolis, S.; Ioakim, C.; Papatheodorou, G.; Ferentinos, G. Evaluation of palaeoenvironmental changes during the last 18,000 years in the Myrtoon basin, SW Aegean Sea. *Palaeogeogr. Palaeoclimatol. Palaeoecol.* **2000**, *156*, 1–17. [\[CrossRef\]](#)
- Geraga, M.; Ioakim, C.; Lykousis, V.; Tsaila-Monopolis, S.; Mylona, G. The high-resolution palaeoclimatic and palaeoceanographic history of the last 24,000 years in the central Aegean Sea, Greece. *Palaeogeogr. Palaeoclimatol. Palaeoecol.* **2010**, *287*, 101–115. [\[CrossRef\]](#)
- Kontakiotis, G.; Mortyn, G.P.; Antonarakou, A.; Drinia, H. Assessing the reliability of foraminiferal Mg/Ca thermometry by comparing field-samples and culture experiments: A review. *Geol. Q.* **2016**, *60*, 547–560. [\[CrossRef\]](#)
- Dämmer, L.K.; de Nooijer, L.; van Sebille, E.; Haak, J.G.; Reichert, G.J. Evaluation of oxygen isotopes and trace elements in planktonic foraminifera from the Mediterranean Sea as recorders of seawater oxygen isotopes and salinity. *Clim. Past* **2020**, *16*, 2401–2414. [\[CrossRef\]](#)
- Wit, J.C.; Reichert, G.J.; Jung, S.J.A.; Kroon, D. Approaches to unravel seasonality in sea surface temperatures using paired single-specimen foraminiferal $\delta^{18}\text{O}$ and Mg/Ca analyses. *Paleoceanography* **2010**, *25*, 58. [\[CrossRef\]](#)

12. Dissard, D.; Reichart, G.J.; Menkes, C.; Mangeas, M.; Frickenhaus, S.; Bijma, J. Mg/Ca, Sr/Ca and stable isotopes from the planktonic foraminifera *T. sacculifer*: Testing a multi-proxy approach for inferring paleotemperature and paleosalinity. *Biogeosciences* **2021**, *18*, 423–439. [[CrossRef](#)]
13. Le Houedec, S.; Erez, J.; Rosenthal, Y. Testing the Influence of Changing Seawater Ca Concentration on Elements/Ca Ratios in Planktic Foraminifera: A Culture Experiment. *Geochem. Geophys. Geosystems* **2021**, *22*, e2020GC009496. [[CrossRef](#)]
14. Hoogakker, B.A.A.; Klinkhammer, G.P.; Elderfield, H.; Rohling, E.J.; Hayward, C. Mg/Ca paleothermometry in high salinity environments. *Earth Planet. Sci. Lett.* **2009**, *284*, 583–589. [[CrossRef](#)]
15. Kısakürek, B.; Eisenhauer, A.; Böhm, F.; Garbe-Schönberg, D.; Erez, J. Controls on shell Mg/Ca and Sr/Ca in cultured planktonic foraminifera, *Globigerinoides ruber* (white). *Earth Planet. Sci. Lett.* **2008**, *273*, 260–269. [[CrossRef](#)]
16. Zarkogiannis, S.; Kontakiotis, G.; Antonarakou, A. Recent planktonic foraminifera population and size response to Eastern Mediterranean hydrography. *Rev. De Micropaléontologie* **2020**, *69*, 100450. [[CrossRef](#)]
17. Kontakiotis, G.; Antonarakou, A.; Mortyn, P.G.; Drinia, H.; Anastasakis, G.; Zarkogiannis, S.; Möbius, J. Morphological recognition of *Globigerinoides ruber* morphotypes and their susceptibility to diagenetic alteration in the eastern Mediterranean Sea. *J. Mar. Syst.* **2017**, *174*, 12–24. [[CrossRef](#)]
18. Thunell, R.C. Distribution of recent planktonic foraminifera in surface sediments of the Mediterranean Sea. *Mar. Micropaleontol.* **1978**, *3*, 147–173. [[CrossRef](#)]
19. Giamali, C.; Kontakiotis, G.; Antonarakou, A.; Koskeridou, E. Ecological Constraints of Plankton Bio-Indicators for Water Column Stratification and Productivity: A Case Study of the Holocene North Aegean Sedimentary Record. *J. Mar. Sci. Eng.* **2021**, *9*, 1249. [[CrossRef](#)]
20. Rebotim, A.; Voelker, A.H.L.; Jonkers, L.; Waniek, J.J.; Meggers, H.; Schiebel, R.; Fraile, I.; Schulz, M.; Kucera, M. Factors controlling the depth habitat of planktonic foraminifera in the subtropical eastern North Atlantic. *Biogeosciences* **2017**, *14*, 827–859. [[CrossRef](#)]
21. Wilke, I.; Meggers, H.; Bickert, T. Depth habitats and seasonal distributions of recent planktic foraminifers in the Canary Islands region (29°N) based on oxygen isotopes. *Deep Sea Res. Part I Oceanogr. Res. Pap.* **2009**, *56*, 89–106. [[CrossRef](#)]
22. Takagi, H.; Kimoto, K.; Fujiki, T.; Saito, H.; Schmidt, C.; Kucera, M.; Moriya, K. Characterizing photosymbiosis in modern planktonic foraminifera. *Biogeosciences* **2019**, *16*, 3377–3396. [[CrossRef](#)]
23. Zarkogiannis, S.D.; Antonarakou, A.; Tripathi, A.; Kontakiotis, G.; Mortyn, P.G.; Drinia, H.; Greaves, M. Influence of surface ocean density on planktonic foraminifera calcification. *Sci. Rep.* **2019**, *9*, 533. [[CrossRef](#)] [[PubMed](#)]
24. Weinkauff, M.F.G.; Kunze, J.G.; Waniek, J.J.; Kučera, M. Seasonal Variation in Shell Calcification of Planktonic Foraminifera in the NE Atlantic Reveals Species-Specific Response to Temperature, Productivity, and Optimum Growth Conditions. *PLoS ONE* **2016**, *11*, e0148363. [[CrossRef](#)] [[PubMed](#)]
25. An, B.; Li, T.; Liu, J.; Sun, H.; Chang, F. Spatial distribution and controlling factors of planktonic foraminifera in the modern western Pacific. *Quat. Int.* **2018**, *468*, 14–23. [[CrossRef](#)]
26. Mallo, M.; Ziveri, P.; Mortyn, P.G.; Schiebel, R.; Grelaud, M. Low planktic foraminiferal diversity and abundance observed in a spring 2013 west-east Mediterranean Sea plankton tow transect. *Biogeosciences* **2017**, *14*, 2245–2266. [[CrossRef](#)]
27. Pujol, C.; Grazzini, C.V. Distribution patterns of live planktic foraminifers as related to regional hydrography and productive systems of the Mediterranean Sea. *Mar. Micropaleontol.* **1995**, *25*, 187–217. [[CrossRef](#)]
28. Kontakiotis, G.; Efstathiou, E.; Zarkogiannis, S.D.; Besiou, E.; Antonarakou, A. Latitudinal Differentiation among Modern Planktonic Foraminiferal Populations of Central Mediterranean: Species-Specific Distribution Patterns and Size Variability. *J. Mar. Sci. Eng.* **2021**, *9*, 551. [[CrossRef](#)]
29. Avnaim-Katav, S.; Herut, B.; Rahav, E.; Katz, T.; Weinstein, Y.; Alkalay, R.; Berman-Frank, I.; Zlatkin, O.; Almogi-Labin, A. Sediment trap and deep sea core-top sediments as tracers of recent changes in planktonic foraminifera assemblages in the southeastern ultra-oligotrophic Levantine Basin. *Deep Sea Res. Part II Top. Stud. Oceanogr.* **2020**, *171*, 104669. [[CrossRef](#)]
30. Schmidt, D.N.; Renaud, S.; Bollmann, J.; Schiebel, R.; Thierstein, H.R. Size distribution of Holocene planktic foraminifer assemblages: Biogeography, ecology and adaptation. *Mar. Micropaleontol.* **2004**, *50*, 319–338. [[CrossRef](#)]
31. Schmidt, D.N.; Thierstein, H.R.; Bollmann, J. The evolutionary history of size variation of planktic foraminiferal assemblages in the Cenozoic. *Palaeogeogr. Palaeoclimatol. Palaeoecol.* **2004**, *212*, 159–180. [[CrossRef](#)]
32. Schmidt, D.N.; Lazarus, D.; Young, J.R.; Kucera, M. Biogeography and evolution of body size in marine plankton. *Earth-Sci. Rev.* **2006**, *78*, 239–266. [[CrossRef](#)]
33. Roussakis, G.; Karageorgis, A.P.; Conispoliatis, N.; Lykousis, V. Last glacial–Holocene sediment sequences in N. Aegean basins: Structure, accumulation rates and clay mineral distribution. *Geo-Mar. Lett.* **2004**, *24*, 97–111. [[CrossRef](#)]
34. Giresse, P.; Buscail, R.; Charrière, B. Late Holocene multisource material input into the Aegean Sea: Depositional and post-depositional processes. *Oceanol. Acta* **2003**, *26*, 657–672. [[CrossRef](#)]
35. Kontakiotis, G. Late Quaternary paleoenvironmental reconstruction and paleoclimatic implications of the Aegean Sea (eastern Mediterranean) based on paleoceanographic indexes and stable isotopes. *Quat. Int.* **2016**, *401*, 28–42. [[CrossRef](#)]
36. Emeis, K.-C.; Struck, U.; Schulz, H.-M.; Rosenberg, R.; Bernasconi, S.; Erlenkeuser, H.; Sakamoto, T.; Martinez-Ruiz, F. Temperature and salinity variations of Mediterranean Sea surface waters over the last 16,000 years from records of planktonic stable oxygen isotopes and alkenone unsaturation ratios. *Palaeogeogr. Palaeoclimatol. Palaeoecol.* **2000**, *158*, 259–280. [[CrossRef](#)]

37. Budillon, F.; Lirer, F.; Iorio, M.; Macri, P.; Sagnotti, L.; Vallefucio, M.; Ferraro, L.; Garziglia, S.; Innangi, S.; Sahabi, M.; et al. Integrated stratigraphic reconstruction for the last 80kyr in a deep sector of the Sardinia Channel (Western Mediterranean). *Deep Sea Res. Part II Top. Stud. Oceanogr.* **2009**, *56*, 725–737. [[CrossRef](#)]
38. Drinia, H.; Antonarakou, A.; Tsourou, T.; Kontakiotis, G.; Psychogiou, M.; Anastasakis, G. Foraminifera eco-biostratigraphy of the southern Evoikos outer shelf, central Aegean Sea, during MIS 5 to present. *Cont. Shelf Res.* **2016**, *126*, 36–49. [[CrossRef](#)]
39. Aksu, A.E.; Jenner, G.; Hiscott, R.N.; İşler, E.B. Occurrence, stratigraphy and geochemistry of Late Quaternary tephra layers in the Aegean Sea and the Marmara Sea. *Mar. Geol.* **2008**, *252*, 174–192. [[CrossRef](#)]
40. Satow, C.; Tomlinson, E.L.; Grant, K.M.; Albert, P.G.; Smith, V.C.; Manning, C.J.; Ottolini, L.; Wulf, S.; Rohling, E.J.; Lowe, J.J.; et al. A new contribution to the Late Quaternary tephrostratigraphy of the Mediterranean: Aegean Sea core LC21. *Quat. Sci. Rev.* **2015**, *117*, 96–112. [[CrossRef](#)]
41. Petrosino, P.; Morabito, S.; Jicha, B.R.; Milia, A.; Sprovieri, M.; Tamburrino, S. Multidisciplinary tephrochronological correlation of marker events in the eastern Tyrrhenian Sea between 48 and 105 ka. *J. Volcanol. Geotherm. Res.* **2016**, *315*, 79–99. [[CrossRef](#)]
42. Wulf, S.; Keller, J.; Satow, C.; Gertisser, R.; Kraml, M.; Grant, K.M.; Appelt, O.; Vakhrameeva, P.; Koutsodendris, A.; Hardiman, M.; et al. Advancing Santorini's tephrostratigraphy: New glass geochemical data and improved marine-terrestrial tephra correlations for the past ~360 kyrs. *Earth-Sci. Rev.* **2020**, *200*, 102964. [[CrossRef](#)]
43. Morabito, S.; Petrosino, P.; Milia, A.; Sprovieri, M.; Tamburrino, S. A multidisciplinary approach for reconstructing the stratigraphic framework of the last 40ka in a bathyal area of the eastern Tyrrhenian Sea. *Glob. Planet. Chang.* **2014**, *123*, 121–138. [[CrossRef](#)]
44. Casford, J.S.L.; Abu-Zied, R.; Rohling, E.J.; Cooke, S.; Fontanier, C.; Leng, M.; Millard, A.; Thomson, J. A stratigraphically controlled multiproxy chronostratigraphy for the eastern Mediterranean. *Paleoceanography* **2007**, *22*, 102964. [[CrossRef](#)]
45. Antonarakou, A.; Kontakiotis, G.; Karageorgis, A.P.; Besiou, E.; Zarkogiannis, S.; Drinia, H.; Mortyn, G.P.; Tripsanas, E. Eco-biostratigraphic advances on late Quaternary geochronology and palaeoclimate: The marginal Gulf of Mexico analogue. *Geol. Q.* **2019**, *63*, 178–191. [[CrossRef](#)]
46. Zouari, S.; Boussetta, S.; Siani, G.; Tisnerat-Laborde, N.; Thil, F.; Kallel, A.; Michel, E.; Kallel, N. Mediterranean faunal evolution and biochronological events during the last 24 kyr. *Mar. Micropaleontol.* **2021**, *165*, 101997. [[CrossRef](#)]
47. Lirer, F.; Foresi, L.M.; Iaccarino, S.M.; Salvatorini, G.; Turco, E.; Cosentino, C.; Sierro, F.J.; Caruso, A. Mediterranean Neogene planktonic foraminifer biozonation and biochronology. *Earth-Sci. Rev.* **2019**, *196*, 102869. [[CrossRef](#)]
48. Pérez-Folgado, M.; Sierro, F.J.; Flores, J.-A.; Cacho, I.; Grimalt, J.O.; Zahn, R.; Shackleton, N.J. Planktonic foraminiferal distribution during the last 70 kyr in the western Mediterranean Sea. *Mar. Micropaleontol.* **2003**, *48*, 49–70. [[CrossRef](#)]
49. Pérez-Folgado, M.; Sierro, F.J.; Flores, J.A.; Grimalt, J.O.; Zahn, R. Paleoclimatic variations in foraminifer assemblages from the Alboran Sea (Western Mediterranean) during the last 150 ka in ODP Site 977. *Mar. Geol.* **2004**, *212*, 113–131. [[CrossRef](#)]
50. Suárez-Ibarra, J.Y.; Petró, S.M.; Frozza, C.F.; Freire, T.M.; Portilho-Ramos, R.D.C.; Pivel, M.A.G. Time-spatial boundaries of bioecozonations (planktonic foraminifera) in the latest Quaternary: A case study from the western South Atlantic. *Rev. Micropaléontol.* **2021**, *73*, 100554. [[CrossRef](#)]
51. Sprovieri, R.; Stefano, E.; Incarbona, A.; Gargano, M. A high-resolution record of the last deglaciation in the Sicily Channel based on foraminifera and calcareous nannofossil quantitative distribution. *Palaeogeogr. Palaeoclimatol. Palaeoecol.* **2003**, *202*, 119–142. [[CrossRef](#)]
52. Sbaffi, L.; Wezel, F.; Kallel, N.; Paterne, M.; Cacho, I.; Ziveri, P.; Shackleton, N. Response of the pelagic environment to palaeoclimatic changes in the central Mediterranean Sea during the Late Quaternary. *Mar. Geol.* **2001**, *178*, 39–62. [[CrossRef](#)]
53. Sbaffi, L.; Wezel, F.C.; Curzi, G.; Zoppi, U. Millennial- to centennial-scale palaeoclimatic variations during Termination I and the Holocene in the central Mediterranean Sea. *Glob. Planet. Chang.* **2004**, *40*, 201–217. [[CrossRef](#)]
54. Di Donato, V.; Esposito, P.; Russo-Ermolli, E.; Scarano, A.; Cheddadi, R. Coupled atmospheric and marine palaeoclimatic reconstruction for the last 35 ka in the Sele Plain–Gulf of Salerno area (southern Italy). *Quat. Int.* **2008**, *190*, 146–157. [[CrossRef](#)]
55. Lirer, F.; Sprovieri, M.; Ferraro, L.; Vallefucio, M.; Capotondi, L.; Cascella, A.; Petrosino, P.; Insinga, D.D.; Pelosi, N.; Tamburrino, S.; et al. Integrated stratigraphy for the Late Quaternary in the eastern Tyrrhenian Sea. *Quat. Int.* **2013**, *292*, 71–85. [[CrossRef](#)]
56. Amore, F.O.; Caffau, M.; Massa, B.; Morabito, S. Late Pleistocene–Holocene paleoclimate and related paleoenvironmental changes as recorded by calcareous nannofossils and planktonic foraminifera assemblages in the southern Tyrrhenian Sea (Cape Palinuro, Italy). *Mar. Micropaleontol.* **2004**, *52*, 255–276. [[CrossRef](#)]
57. Jorissen, F.J.; Asioli, A.; Borsetti, A.M.; Capotondi, L.; de Visser, J.P.; Hilgen, F.J.; Rohling, E.J.; van der Borg, K.; Vergnaud Grazzini, C.; Zachariasse, W.J. Late Quaternary central Mediterranean biochronology. *Mar. Micropaleontol.* **1993**, *21*, 169–189. [[CrossRef](#)]
58. Capotondi, L.; Maria Borsetti, A.; Morigi, C. Foraminiferal ecozones, a high resolution proxy for the late Quaternary biochronology in the central Mediterranean Sea. *Mar. Geol.* **1999**, *153*, 253–274. [[CrossRef](#)]
59. Asioli, A.; Trincardi, F.; Lowe, J.J.; Ariztegui, D.; Langone, L.; Oldfield, F. Sub-millennial scale climatic oscillations in the central Adriatic during the Lateglacial: Palaeoceanographic implications. *Quat. Sci. Rev.* **2001**, *20*, 1201–1221. [[CrossRef](#)]
60. Asioli, A.; Trincardi, F.; Lowe, J.J.; Oldfield, F. Short-term climate changes during the Last Glacial–Holocene transition: Comparison between Mediterranean records and the GRIP event stratigraphy. *J. Quat. Sci.* **1999**, *14*, 373–381. [[CrossRef](#)]
61. Siani, G.; Paterne, M.; Colin, C. Late glacial to Holocene planktic foraminifera bioevents and climatic record in the South Adriatic Sea. *J. Quat. Sci.* **2010**, *25*, 808–821. [[CrossRef](#)]

62. Principato, M.S.; Giunta, S.; Corselli, C.; Negri, A. Late Pleistocene–Holocene planktonic assemblages in three box-cores from the Mediterranean Ridge area (west–southwest of Crete): Palaeoecological and palaeoceanographic reconstruction of sapropel S1 interval. *Palaeogeogr. Palaeoclimatol. Palaeoecol.* **2003**, *190*, 61–77. [CrossRef]
63. Geraga, M.; Mylona, G.; Tsaila-Monopoli, S.; Papatheodorou, G.; Ferentinos, G. Northeastern Ionian Sea: Palaeoceanographic variability over the last 22 ka. *J. Mar. Syst.* **2008**, *74*, 623–638. [CrossRef]
64. Louvari, M.A.; Drinia, H.; Kontakiotis, G.; Di Bella, L.; Antonarakou, A.; Anastasakis, G. Impact of latest-glacial to Holocene sea-level oscillations on central Aegean shelf ecosystems: A benthic foraminiferal palaeoenvironmental assessment of South Evoikos Gulf, Greece. *J. Mar. Syst.* **2019**, *199*, 103181. [CrossRef]
65. Lykousis, V.; Chronis, G.; Tselepidis, A.; Price, N.B.; Theocharis, A.; Siokou-Frangou, I.; Van Wambeke, F.; Danovaro, R.; Stavrakakis, S.; Duineveld, G.; et al. Major outputs of the recent multidisciplinary biogeochemical researches undertaken in the Aegean Sea. *J. Mar. Syst.* **2002**, *33–34*, 313–334. [CrossRef]
66. Ignatiades, L.; Psarra, S.; Zervakis, V.; Pagou, K.; Souvermezoglou, E.; Assimakopoulou, G.; Gotsis-Skretas, O. Phytoplankton size-based dynamics in the Aegean Sea (Eastern Mediterranean). *J. Mar. Syst.* **2002**, *36*, 11–28. [CrossRef]
67. Price, N.B.; Lindsay, F.S.; Pates, J.M. The biogeochemistry of major elements of the suspended particulate matter of the Cretan Sea. *Prog. Oceanogr.* **1999**, *44*, 677–699. [CrossRef]
68. Psarra, S.; Tselepidis, A.; Ignatiades, L. Primary productivity in the oligotrophic Cretan Sea (NE Mediterranean): Seasonal and interannual variability. *Prog. Oceanogr.* **2000**, *46*, 187–204. [CrossRef]
69. Tselepidis, A.; Zervakis, V.; Polychronaki, T.; Danovaro, R.; Chronis, G. Distribution of nutrients and particulate organic matter in relation to the prevailing hydrographic features of the Cretan Sea (NE Mediterranean). *Prog. Oceanogr.* **2000**, *46*, 113–142. [CrossRef]
70. Karageorgis, A.P.; Gardner, W.D.; Georgopoulos, D.; Mishonov, A.V.; Krasakopoulou, E.; Anagnostou, C. Particle dynamics in the Eastern Mediterranean Sea: A synthesis based on light transmission, PMC, and POC archives (1991–2001). *Deep Sea Res. Part I Oceanogr. Res. Pap.* **2008**, *55*, 177–202. [CrossRef]
71. Theocharis, A.; Georgopoulos, D.; Lascaratos, A.; Nittis, K. Water masses and circulation in the central region of the Eastern Mediterranean: Eastern Ionian, South Aegean and Northwest Levantine, 1986–1987. *Deep Sea Res. Part II Top. Stud. Oceanogr.* **1993**, *40*, 1121–1142. [CrossRef]
72. Papanikolaou, D.; Alexandri, M.; Nomikou, P.; Ballas, D. Morphotectonic structure of the western part of the North Aegean Basin based on swath bathymetry. *Mar. Geol.* **2002**, *190*, 465–492. [CrossRef]
73. Poulos, S.E. Origin and distribution of the terrigenous component of the unconsolidated surface sediment of the Aegean floor: A synthesis. *Cont. Shelf Res.* **2009**, *29*, 2045–2060. [CrossRef]
74. Roether, W.; Klein, B.; Manca, B.B.; Theocharis, A.; Kioroglou, S. Transient Eastern Mediterranean deep waters in response to the massive dense-water output of the Aegean Sea in the 1990s. *Prog. Oceanogr.* **2007**, *74*, 540–571. [CrossRef]
75. Theocharis, A.; Balopoulos, E.; Kioroglou, S.; Kontoyiannis, H.; Iona, A. A synthesis of the circulation and hydrography of the South Aegean Sea and the Straits of the Cretan Arc (March 1994–January 1995). *Prog. Oceanogr.* **1999**, *44*, 469–509. [CrossRef]
76. Pinaridi, N.; Zavatarelli, M.; Adani, M.; Coppini, G.; Fratianni, C.; Oddo, P.; Simoncelli, S.; Tonani, M.; Lyubartsev, V.; Dobricic, S.; et al. Mediterranean Sea large-scale low-frequency ocean variability and water mass formation rates from 1987 to 2007: A retrospective analysis. *Prog. Oceanogr.* **2015**, *132*, 318–332. [CrossRef]
77. Zervakis, V.; Georgopoulos, D.; Drakopoulos, P.G. The role of the North Aegean in triggering the recent Eastern Mediterranean climatic changes. *J. Geophys. Res. Ocean.* **2000**, *105*, 26103–26116. [CrossRef]
78. Lykousis, V. Subaqueous bedforms on the Cyclades Plateau (NE Mediterranean)—Evidence of Cretan Deep Water Formation? *Cont. Shelf Res.* **2001**, *21*, 495–507. [CrossRef]
79. Mercone, D.; Thomson, J.; Croudace, I.W.; Siani, G.; Paterne, M.; Troelstra, S. Duration of S1, the most recent sapropel in the eastern Mediterranean Sea, as indicated by accelerator mass spectrometry radiocarbon and geochemical evidence. *Paleoceanography* **2000**, *15*, 336–347. [CrossRef]
80. Triantaphyllou, M.V. Coccolithophore assemblages during the Holocene Climatic Optimum in the NE Mediterranean (Aegean and northern Levantine Seas, Greece): Paleoceanographic and paleoclimatic implications. *Quat. Int.* **2014**, *345*, 56–67. [CrossRef]
81. Reimer, P.J.; McCormac, F.G. Marine Radiocarbon Reservoir Corrections for the Mediterranean and Aegean Seas. *Radiocarbon* **2016**, *44*, 159–166. [CrossRef]
82. Stuiver, M.; Reimer, P.J.; Reimer, R.W. CALIB 8.2 [WWW Program]. 2021, Volume 13. Available online: <http://calib.org> (accessed on 1 January 2023).
83. Zarkogiannis, S.D.; Kontakiotis, G.; Gkaniatsa, G.; Kuppili, V.S.C.; Marathe, S.; Wanelik, K.; Lianou, V.; Besiou, E.; Makri, P.; Antonarakou, A. An Improved Cleaning Protocol for Foraminiferal Calcite from Unconsolidated Core Sediments: HyPerCal—A New Practice for Micropaleontological and Paleoclimatic Proxies. *J. Mar. Sci. Eng.* **2020**, *8*, 998. [CrossRef]
84. Capotondi, L.; Soroldoni, E.; Principato, M.S.; Corselli, C. Late Quaternary planktonic foraminiferal distributions: Problems related to size fraction. In Proceedings of the First Italian Meeting on Environmental Micropaleontology, Urbino, Italy, 4–6 June 2002; Coccioni, R.G.S., Lirer, F., Eds.; Grzybowski Foundation, Special Publication: Krakow, Poland, 2004; Volume 9, pp. 1–6.
85. Fatela, F.; Taborda, R. Confidence limits of species proportions in microfossil assemblages. *Mar. Micropaleontol.* **2002**, *45*, 169–174. [CrossRef]
86. Hemleben, C.; Anderson, O.R.; Spindler, M. *Modern Planktonic Foraminifera*; Springer-Verlag: New York, NY, USA, 1989.

87. Brummer, G.J.A.; Kučera, M. Taxonomic review of living planktonic foraminifera. *J. Micropalaeontol.* **2022**, *41*, 29–74. [[CrossRef](#)]
88. Kozanoglou, C.; Triantaphyllou, M.V.; Geraga, M.; Rousakis, G.; Papatheodorou, G.; Arabas, A.; Dimiza, M.D.; Gogou, A. A high-resolution study of planktonic foraminifera during the Holocene at the Tilos-Symi sea basin in the SE Aegean Sea. *Holocene* **2023**, *33*, 1317–1332. [[CrossRef](#)]
89. Rohling, E.J.; Jorissen, F.J.; Grazzini, C.V.; Zachariasse, W.J. Northern Levantine and Adriatic Quaternary planktic foraminifera; Reconstruction of paleoenvironmental gradients. *Mar. Micropaleontol.* **1993**, *21*, 191–218. [[CrossRef](#)]
90. Triantaphyllou, M.V.; Ziveri, P.; Gogou, A.; Marino, G.; Lykousis, V.; Bouloubassi, I.; Emeis, K.C.; Kouli, K.; Dimiza, M.; Rosell-Melé, A.; et al. Late Glacial–Holocene climate variability at the south-eastern margin of the Aegean Sea. *Mar. Geol.* **2009**, *266*, 182–197. [[CrossRef](#)]
91. Essallami, L.; Sicre, M.A.; Kallel, N.; Labeyrie, L.; Siani, G. Hydrological changes in the Mediterranean Sea over the last 30,000 years. *Geochim. Geophys. Geosystems* **2007**, *8*, 59. [[CrossRef](#)]
92. Rouis-Zargouni, I.; Turon, J.-L.; Londeix, L.; Essallami, L.; Kallel, N.; Sicre, M.-A. Environmental and climatic changes in the central Mediterranean Sea (Siculo–Tunisian Strait) during the last 30ka based on dinoflagellate cyst and planktonic foraminifera assemblages. *Palaeogeogr. Palaeoclimatol. Palaeoecol.* **2010**, *285*, 17–29. [[CrossRef](#)]
93. Zachariasse, W.; Jorissen, F.; Perissoratis, C.; Rohling, E.; Tsapralis, V. Late Quaternary foraminiferal changes and the nature of sapropel S1 in Skopelos Basin. In Proceedings of the 5th Hellenic Symposium of Oceanography and Fisheries, Kavala, Greece, 27 July 1997; pp. 391–394.
94. Hayes, A.; Rohling, E.J.; De Rijk, S.; Kroon, D.; Zachariasse, W.J. Mediterranean planktonic foraminiferal faunas during the last glacial cycle. *Mar. Geol.* **1999**, *153*, 239–252. [[CrossRef](#)]
95. Casford, J.S.L.; Rohling, E.J.; Abu-Zied, R.; Cooke, S.; Fontanier, C.; Leng, M.; Lykousis, V. Circulation changes and nutrient concentrations in the late Quaternary Aegean Sea: A nonsteady state concept for sapropel formation. *Paleoceanography* **2002**, *17*, 14-1–14-11. [[CrossRef](#)]
96. Rohling, E.J.; Jorissen, F.J.; De Stigter, H.C. 200 Year interruption of Holocene sapropel formation in the Adriatic Sea. *J. Micropalaeontol.* **1997**, *16*, 97–108. [[CrossRef](#)]
97. De Rijk, S.; Hayes, A.; Rohling, E.J. Eastern Mediterranean sapropel S1 interruption: An expression of the onset of climatic deterioration around 7 ka BP. *Mar. Geol.* **1999**, *153*, 337–343. [[CrossRef](#)]
98. Papanikolaou, D.; Nomikou, P. Tectonic structure and volcanic centers at the eastern edge of the aegean volcanic arc around Nisyros island. *Bull. Geol. Soc. Greece* **2001**, *34*, 289–296. [[CrossRef](#)]
99. Pujol, C.; Vergnaud Grazzini, C. Palaeoceanography of the last deglaciation in the Alboran Sea (western Mediterranean). Stable isotopes and planktonic foraminiferal records. *Mar. Micropaleontol.* **1989**, *15*, 153–179. [[CrossRef](#)]
100. Rohling, E.J.; Gieskes, W.W.C. Late Quaternary changes in Mediterranean intermediate water density and formation rate. *Paleoceanography* **1989**, *4*, 531–545. [[CrossRef](#)]
101. Cacho, I.; Grimalt, J.O.; Canals, M.; Sbaffi, L.; Shackleton, N.J.; Schönfeld, J.; Zahn, R. Variability of the western Mediterranean Sea surface temperature during the last 25,000 years and its connection with the Northern Hemisphere climatic changes. *Paleoceanography* **2001**, *16*, 40–52. [[CrossRef](#)]
102. Buccheri, G.; Capretto, G.; Di Donato, V.; Esposito, P.; Ferruzza, G.; Pescatore, T.; Russo Ermolli, E.; Senatore, M.R.; Sprovieri, M.; Bertoldo, M.; et al. A high resolution record of the last deglaciation in the southern Tyrrhenian Sea: Environmental and climatic evolution. *Mar. Geol.* **2002**, *186*, 447–470. [[CrossRef](#)]
103. Carboni, M.G.; Bergamin, L.; Di Bella, L.; Landini, B.; Manfra, L.; Vesica, P. Late Quaternary paleoclimatic and paleoenvironmental changes in the Tyrrhenian Sea. *Quat. Sci. Rev.* **2005**, *24*, 2069–2082. [[CrossRef](#)]
104. Paterne, M.; Kallel, N.; Labeyrie, L.; Vautravers, M.; Duplessy, J.-C.; Rossignol-Strick, M.; Cortijo, E.; Arnold, M.; Fontugne, M. Hydrological relationship between the North Atlantic Ocean and the Mediterranean Sea during the past 15–75 kyr. *Paleoceanography* **1999**, *14*, 626–638. [[CrossRef](#)]
105. Bordon, A.; Peyron, O.; Lézine, A.-M.; Brewer, S.; Fouache, E. Pollen-inferred Late-Glacial and Holocene climate in southern Balkans (Lake Maliq). *Quat. Int.* **2009**, *200*, 19–30. [[CrossRef](#)]
106. Larocque, I.; Finsinger, W. Late-glacial chironomid-based temperature reconstructions for Lago Piccolo di Avigliana in the southwestern Alps (Italy). *Palaeogeogr. Palaeoclimatol. Palaeoecol.* **2008**, *257*, 207–223. [[CrossRef](#)]
107. Dormoy, I.; Peyron, O.; Combourieu Nebout, N.; Goring, S.; Kotthoff, U.; Magny, M.; Pross, J. Terrestrial climate variability and seasonality changes in the Mediterranean region between 15 000 and 4000 years BP deduced from marine pollen records. *Clim. Past* **2009**, *5*, 615–632. [[CrossRef](#)]
108. Björck, S.; Walker, M.J.C.; Cwynar, L.C.; Johnsen, S.; Knudsen, K.-L.; Lowe, J.J.; Wohlfarth, B. An event stratigraphy for the Last Termination in the North Atlantic region based on the Greenland ice-core record: A proposal by the INTIMATE group. *J. Quat. Sci.* **1998**, *13*, 283–292. [[CrossRef](#)]
109. Peyron, O.; Bégeot, C.; Brewer, S.; Heiri, O.; Magny, M.; Millet, L.; Ruffaldi, P.; Van Campo, E.; Yu, G. Lateglacial climate in the Jura mountains (France) based on different quantitative reconstruction approaches from pollen, lake-levels, and chironomids. *Quat. Res.* **2005**, *64*, 197–211. [[CrossRef](#)]
110. Rasmussen, S.O.; Andersen, K.K.; Svensson, A.M.; Steffensen, J.P.; Vinther, B.M.; Clausen, H.B.; Siggaard-Andersen, M.L.; Johnsen, S.J.; Larsen, L.B.; Dahl-Jensen, D.; et al. A new Greenland ice core chronology for the last glacial termination. *J. Geophys. Res. Atmos.* **2006**, *111*, 1348. [[CrossRef](#)]

111. Gogou, A.; Bouloubassi, I.; Lykousis, V.; Arnaboldi, M.; Gaitani, P.; Meyers, P.A. Organic geochemical evidence of Late Glacial–Holocene climate instability in the North Aegean Sea. *Palaeogeogr. Palaeoclimatol. Palaeoecol.* **2007**, *256*, 1–20. [[CrossRef](#)]
112. De Lange, G.J.; Thomson, J.; Reitz, A.; Slomp, C.P.; Speranza Principato, M.; Erba, E.; Corselli, C. Synchronous basin-wide formation and redox-controlled preservation of a Mediterranean sapropel. *Nat. Geosci.* **2008**, *1*, 606–610. [[CrossRef](#)]
113. Alley, R.B.; Mayewski, P.A.; Sowers, T.; Stuiver, M.; Taylor, K.C.; Clark, P.U. Holocene climatic instability: A prominent, widespread event 8200 yr ago. *Geology* **1997**, *25*, 483–486. [[CrossRef](#)]
114. Ariztegui, D.; Asioli, A.; Lowe, J.J.; Trincardi, F.; Vigliotti, L.; Tamburini, F.; Chondrogianni, C.; Accorsi, C.A.; Bandini Mazzanti, M.; Mercuri, A.M.; et al. Palaeoclimate and the formation of sapropel S1: Inferences from Late Quaternary lacustrine and marine sequences in the central Mediterranean region. *Palaeogeogr. Palaeoclimatol. Palaeoecol.* **2000**, *158*, 215–240. [[CrossRef](#)]
115. Rohling, E.; Mayewski, P.; Abu-Zied, R.; Casford, J.; Hayes, A. Holocene atmosphere–ocean interactions: Records from Greenland and the Aegean Sea. *Clim. Dyn.* **2002**, *18*, 587–593. [[CrossRef](#)]
116. Bazzicalupo, P.; Maiorano, P.; Girone, A.; Marino, M.; Combourieu-Nebout, N.; Pelosi, N.; Salgueiro, E.; Incarbona, A. Holocene climate variability of the Western Mediterranean: Surface water dynamics inferred from calcareous plankton assemblages. *Holocene* **2020**, *30*, 691–708. [[CrossRef](#)]
117. Casford, J.S.L.; Rohling, E.J.; Abu-Zied, R.H.; Fontanier, C.; Jorissen, F.J.; Leng, M.J.; Schmiedl, G.; Thomson, J. A dynamic concept for eastern Mediterranean circulation and oxygenation during sapropel formation. *Palaeogeogr. Palaeoclimatol. Palaeoecol.* **2003**, *190*, 103–119. [[CrossRef](#)]
118. Triantaphyllou, M.V.; Gogou, A.; Dimiza, M.D.; Kostopoulou, S.; Parinos, C.; Roussakis, G.; Geraga, M.; Bouloubassi, I.; Fleitmann, D.; Zervakis, V.; et al. Holocene Climatic Optimum centennial-scale paleoceanography in the NE Aegean (Mediterranean Sea). *Geo-Mar. Lett.* **2016**, *36*, 51–66. [[CrossRef](#)]
119. Kotthoff, U.; Müller, U.C.; Pross, J.; Schmiedl, G.; Lawson, I.T.; van de Schootbrugge, B.; Schulz, H. Lateglacial and Holocene vegetation dynamics in the Aegean region: An integrated view based on pollen data from marine and terrestrial archives. *Holocene* **2008**, *18*, 1019–1032. [[CrossRef](#)]
120. Kotthoff, U.; Pross, J.; Müller, U.C.; Peyron, O.; Schmiedl, G.; Schulz, H.; Bordon, A. Climate dynamics in the borderlands of the Aegean Sea during formation of sapropel S1 deduced from a marine pollen record. *Quat. Sci. Rev.* **2008**, *27*, 832–845. [[CrossRef](#)]

Disclaimer/Publisher’s Note: The statements, opinions and data contained in all publications are solely those of the individual author(s) and contributor(s) and not of MDPI and/or the editor(s). MDPI and/or the editor(s) disclaim responsibility for any injury to people or property resulting from any ideas, methods, instructions or products referred to in the content.